Measurements of strange and multi-strange hadrons elliptic flow in isobar collisions at RHIC by STAR

V. Bairathi (for the STAR Collaboration)

Instituto de Alta Investigación, Universidad de Tarapacá,
Casilla 7D, Arica 1000000, Chile

November 6, 2023

Abstract

We present measurements of elliptic flow (v_2) of K_s^0, Λ, $\bar{\Lambda}$, ϕ, Ξ^-, $\overline{\Xi}^+$, and Ω^-+$\overline{\Omega}^+$ at mid-rapidity ($|\eta| < 1.0$) in isobar collisions ($^{96}_{44}$Ru+$^{96}_{44}$Ru and $^{96}_{40}$Zr+$^{96}_{40}$Zr) at $\sqrt{s_{\mathrm{NN}}}$ = 200 GeV. The centrality and transverse momentum (p_{T}) dependence of elliptic flow is presented. The number of constituent quark (NCQ) scaling of v_2 in isobar collisions is discussed. p_T-integrated elliptic flow ($\langle v_2 \rangle$) is observed to increase from central to peripheral collisions. The ratio of $\langle v_2 \rangle$ between the two isobars shows a deviation from unity for strange hadrons (K_s^0, Λ and $\bar{\Lambda}$) indicating a difference in nuclear structure and deformation. A system size dependence of strange hadron v_2 at high p_T is observed among Ru+Ru, Zr+Zr, Cu+Cu, Au+Au, and U+U systems. A multi-phase transport (AMPT) model with string melting (SM) describes the experimental data well in the measured p_{T} range for isobar collisions at $\sqrt{s_{\mathrm{NN}}} = 200$ GeV.

1 Introduction

Predictions from quantum chromodynamics (QCD) suggest the formation of a deconfined state of quarks and gluons at sufficiently high temperature and energy density called quark-gluon plasma (QGP) [1, 2, 3]. Many studies in heavy-ion collisions at the Relativistic Heavy Ion Collider (RHIC) [4, 5, 6, 7] and the Large Hadron Collider (LHC) [8, 9, 10] have reported the presence of such a medium dominated by the partonic degrees of freedom, which motivates the study of the QGP. The collective flow of produced particles is one of the key observables to probe the QGP medium. It is quantified by the coefficients in the Fourier expansion of azimuthal angle distribution of produced particles with respect to the symmetry planes [11]. This azimuthal anisotropic flow of produced particles indicates hydrodynamic and collective behavior of the strongly interacting matter during the collision [12]. It arises due to spatial anisotropy of the initial overlap geometry of the colliding nuclei as a consequence of inhomogeneous initial energy deposition and fluctuations of nucleon positions in heavy-ion collisions. The initial spatial anisotropies are converted into final state momentum anisotropies through multi-particle interactions among partons during the medium evolution.

The STAR experiment at RHIC collected data in the year 2018 by colliding isobars (Ru+Ru and Zr+Zr) at $\sqrt{s_{\mathrm{NN}}} = 200$ GeV. It was mainly focused at measuring the charge separation along the magnetic field, driven by a phenomenon called the Chiral Magnetic Effect (CME) [13]. The two isobar nuclei have the same atomic mass number but differ in nuclear deformation parameters, and flow measurements are highly sensitive to them. Moreover, the measurement of strange and multi-strange hadrons flow is an excellent probe for understanding the initial state anisotropies due to their small hadronic interaction cross-section compared to light hadrons. Therefore, a systematic study of the anisotropic flow of strange and multi-strange hadrons could be crucial to understanding the effect of initial states in the isobar collisions.

2 Dataset and analysis method

In these proceedings, we report v_2 of K_s^0, Λ, $\bar{\Lambda}$, ϕ, Ξ^-, $\overline{\Xi}^+$, and $\Omega^-+\overline{\Omega}^+$ at mid-rapidity ($|\eta| < 1.0$) in Ru+Ru and Zr+Zr collisions at $\sqrt{s_{\mathrm{NN}}} = 200$ GeV. A total of ~650 M minimum bias good events for each system out of the total 1.8 B (2 B) events of Ru+Ru (Zr+Zr) collisions are used for this analysis. The above particles are reconstructed using the invariant mass technique through their hadronic decay channels. The combinatorial background is constructed using a rotational method for weakly decaying hadrons, while for ϕ-mesons event mixing technique is used [14, 15]. The η-sub event plane method with a η-gap of 0.1 between the two sub-events (-1.0 < η < -0.05 and 0.05 < η < 1.0) is used to calculate v_2 of these hadrons [11]. The azimuthal dependence of the particle yield can be expanded in terms of a Fourier series with respect to the event plane angle [11]:

$$E\frac{d^3N}{dp^3} = \frac{d^2N}{2\pi p_T dp_T dy}\left(1 + 2\sum_{n=1}^{\infty} v_n(p_T, y)\cos[n(\phi - \Psi_n)]\right), \tag{1}$$

where p_T and y are the transverse momentum and rapidity of the particles. The second-order Fourier coefficient v_2, known as elliptic flow, is particularly sensitive to the initial geometry of the collisions and the properties of the medium in the heavy-ion collisions. Ψ_n is the orientation of the nth-order event plane. It is reconstructed from the azimuthal distribution of final-state particles as,

$$\psi_n = \frac{1}{n}\tan^{-1}\frac{\sum_i w_i sin(n\phi_i)}{\sum_i w_i \cos(n\phi_i)}, \tag{2}$$

where, ϕ_i and w_i represent azimuthal angle and weight for the i^{th} particle, respectively. In order to minimize the effects of non-flow correlations, only charged particle tracks with a transverse momentum range of $0.2 < p_{\mathrm{T}} < 2.0$ GeV/c are selected to reconstruct the event plane angle. Since the event plane angle is estimated in finite multiplicity, flow coefficients need to be corrected for the event plane resolution. Therefore, the v_n measured with respect to the reconstructed event plane is divided by the event plane angle resolution to get the final flow coefficients as,

$$v_n = \frac{v_n^{obs}}{\langle\cos\left[n(\psi_n^A - \psi_n^B)\right]\rangle}. \tag{3}$$

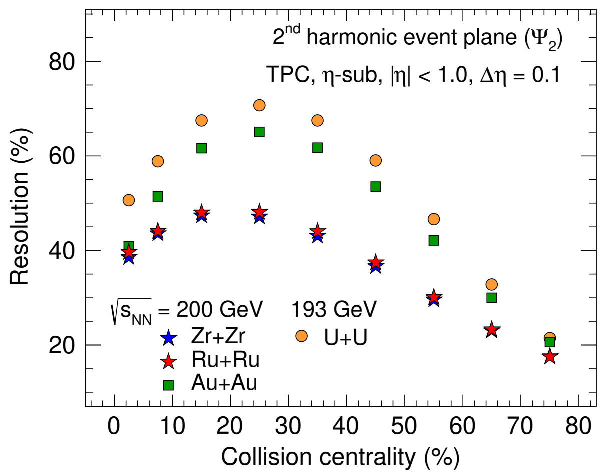

Figure 1: 2^{nd}-order harmonic event plane angle resolution as a function of centrality.

Figure 1 shows the event plane resolution as a function of centrality at mid-rapidity ($|\eta| < 1.0$) in Ru+Ru and Zr+Zr collisions at $\sqrt{s_{\mathrm{NN}}} = 200$ GeV. For comparison, event plane resolution from the published results in Au+Au collisions at $\sqrt{s_{\mathrm{NN}}} = 200$ GeV and

U+U collisions at $\sqrt{s_{\mathrm{NN}}} = 193$ GeV are also shown. The event plane resolution is better for systems with more multiplicity and the number of participants. It shows similar centrality dependence in all the systems.

3 Results

3.1 p_T dependence of v_2

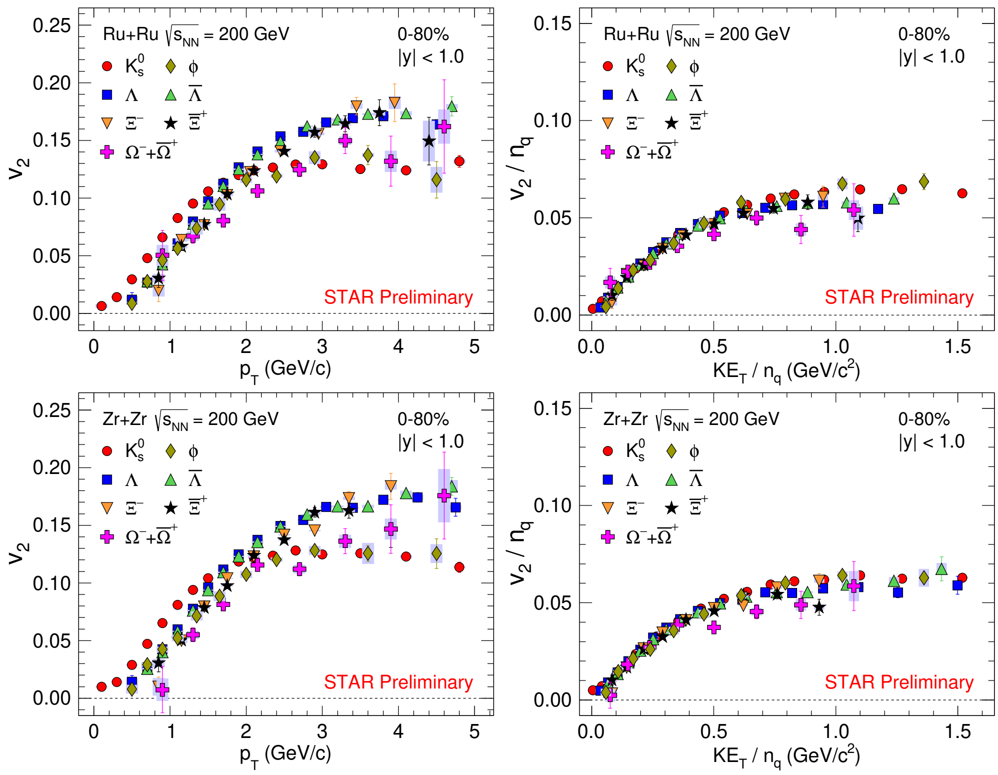

Figure 2: v_2 as a function of p_T for K_s^0, Λ, $\bar{\Lambda}$, ϕ, Ξ^-, $\overline{\Xi}^+$, and Ω^-+$\overline{\Omega}^+$ at mid-rapidity in minimum bias Ru+Ru collisions (top left panel) and Zr+Zr collisions (bottom left panel) at $\sqrt{s_{\mathrm{NN}}} = 200$ GeV. NCQ scaled v_2 vs transverse kinetic energy (KE_T/n_q) is also shown for Ru+Ru collisions (top right panel) and Zr+Zr collisions (bottom right panel) at $\sqrt{s_{\mathrm{NN}}}$ = 200 GeV. The bands represent systematic uncertainties.

Figure 2 shows strange and multi-strange hadrons v_2 as function of p_T for minimum bias (0-80%) Ru+Ru and Zr+Zr collisions at $\sqrt{s_{\mathrm{NN}}} = 200$ GeV. v_2 follows a particle mass ordering indicating hydrodynamic behavior of the medium at low p_T. Whereas, at intermediate p_T, it shows a splitting between baryons and mesons, which suggests the formation of QGP medium in isobar collisions at $\sqrt{s_{\mathrm{NN}}} = 200$ GeV. A similar transverse momentum dependence of v_2 is observed for both Ru+Ru and Zr+Zr collisions.

Figure 2 also shows v_2 of strange and multi-strange hadrons scaled by the number of constituent quarks n_q in minimum bias Ru+Ru and Zr+Zr collisions at $\sqrt{s_{\rm NN}} = 200$ GeV. The results are presented as a function of transverse kinetic energy to remove the effect of particle mass at low p_T. It is defined as $KE_T = m_T - m_0$, where m_T is the transverse mass ($\sqrt{p_T^2 + m_0^2}$) and m_0 is rest mass of the particle. The v_2 of strange and multi-strange hadrons follows the number of constituent quarks (NCQ) scaling with $\pm$10% uncertainty in both collision systems. The NCQ scaling of v_2 suggests the formation and collective behavior of the QGP medium. It also indicates that quark coalescence is the dominant mechanism of particle production.

3.2 Centrality dependence of v_2

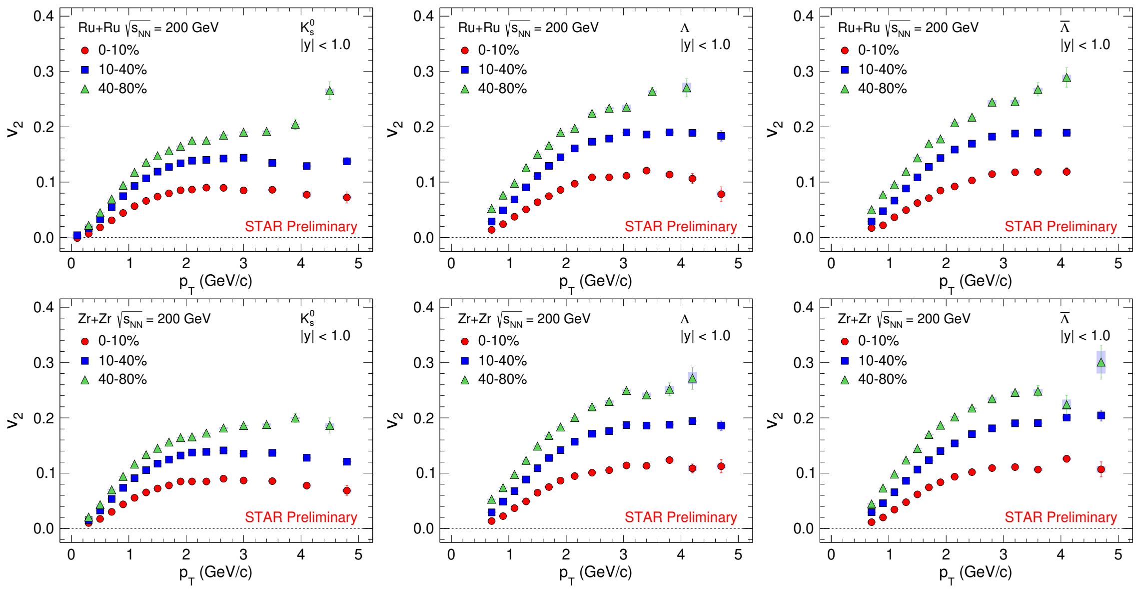

Figure 3: $v_2(p_T)$ of strange hadrons at mid-rapidity in Ru+Ru (top panels) and Zr+Zr (bottom panels) collisions at $\sqrt{s_{\rm NN}} = 200$ GeV for centrality 0-10%, 10-40%, and 40-80%. The bands represent systematic uncertainties.

Figures 3 and 4 show $v_2(p_T)$ of strange and multi-strange hadrons for various centrality intervals in Ru+Ru and Zr+Zr collisions at $\sqrt{s_{\rm NN}} = 200$ GeV. A strong centrality dependence is observed for all the particles studied in both the isobar systems. The magnitude of v_2 increases from central (0-10%) to peripheral (40-80%) collisions, which indicate the effect of initial eccentricity in isobar collisions at $\sqrt{s_{\rm NN}} = 200$ GeV.

Figure 5 shows p_T-integrated v_2 of strange hadrons as a function of centrality in Ru+Ru and Zr+Zr collisions at $\sqrt{s_{\rm NN}} = 200$ GeV. The ratio of v_2 in Ru+Ru to Zr+Zr collisions is also shown in the bottom panels of Fig. 5 and fitted with a constant polynomial function for mid-central collisions (20-50%). About $\sim$2% deviation from unity with a significance of 6.25σ for $\Lambda(\bar{\Lambda})$ and 1.83σ for K_s^0 is observed, which is consistent with the expectation

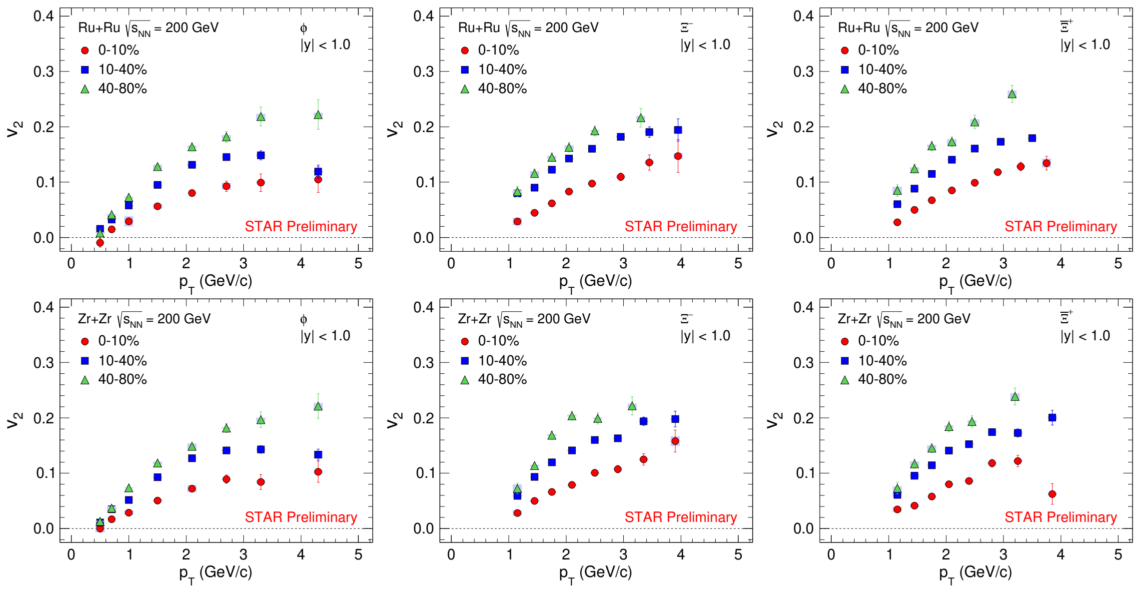

Figure 4: $v_2(p_T)$ of multi-strange hadrons at mid-rapidity in Ru+Ru (top panels) and Zr+Zr (bottom panels) at $\sqrt{s_{\rm NN}}$ = 200 GeV for centrality 0-10%, 10-40%, and 40-80%. The bands represent systematic uncertainties.

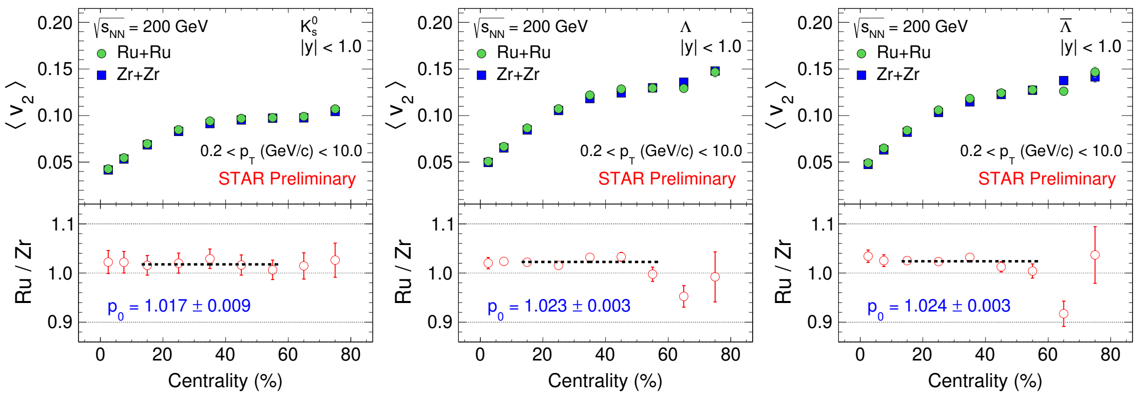

Figure 5: p_T-integrated v_2 vs centrality for strange hadrons at mid-rapidity in Ru+Ru and Zr+Zr collisions at $\sqrt{s_{\rm NN}}$ = 200 GeV. The bottom panels also show the ratio of v_2 between Ru and Zr. The error bars represent statistical and systematic uncertainties added in quadrature.

from the difference between the nuclear structures of the two isobar nuclei [16].

3.3 System size dependence

Figure 6 shows v_2 of strange hadrons in Ru+Ru and Zr+Zr collisions at $\sqrt{s_{\rm NN}} = 200$ GeV compared to the published results from the STAR experiment at RHIC in Cu+Cu, Au+Au, and U+U collisions [17, 18, 19]. A system size dependence of v_2 is observed for p_T above ~1.5 GeV/c. The v_2 follow the hierarchy $v_2^{\rm Cu} < v_2^{\rm Ru/Zr} < v_2^{\rm Au} < v_2^{\rm U}$. Its magnitude increases with increase in the system size.

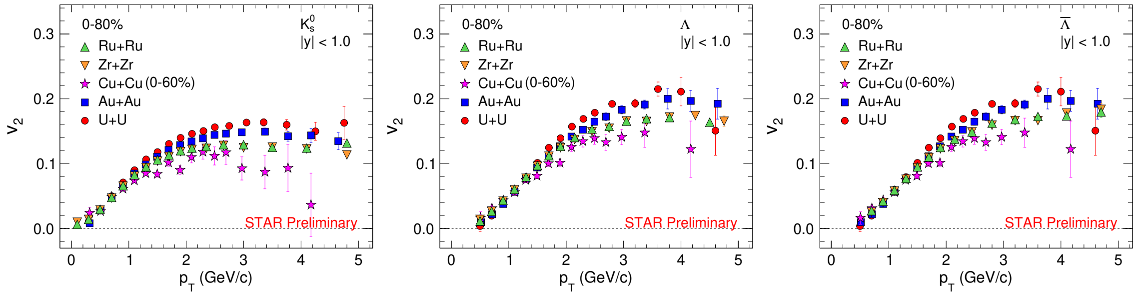

Figure 6: Strange hadron v_2 as a function of p_T at mid-rapidity in minimum bias Ru+Ru and Zr+Zr collisions at $\sqrt{s_{\rm NN}} = 200$ GeV compared to Cu+Cu, Au+Au, and U+U collisions [17, 18, 19]. The error bars represent statistical and systematic uncertainties added in quadrature.

3.4 Model comparison

The AMPT model is a hybrid Monte Carlo event generator extensively used to study relativistic heavy-ion collisions [20]. The colliding nuclei in AMPT are modeled according to a deformed Wood-Saxon distribution with nuclear radius given by,

$$R(\theta, \phi) = R_0 \left[1 + \beta_2 Y_{2,0}(\theta, \phi) + \beta_3 Y_{3,0}(\theta, \phi)\right]. \quad (4)$$

R_0 represents the radius parameter, β_2 and β_3 are the quadrupole and octupole deformities, and $Y_{l,m}(\theta, \phi)$ are the spherical harmonics. We studied two different cases of Wood-Saxon parameters for Ru+Ru and Zr+Zr collisions at $\sqrt{s_{\rm NN}} = 200$ GeV, as shown in Table 1 [21]. About 9 million minimum bias events for Ru+Ru and Zr+Zr collisions at $\sqrt{s_{\rm NN}} = 200$ GeV with parton-parton cross-section three mb have been analyzed for each case.

Figure 7 and 8 show v_2 of strange and multi-strange hadrons in minimum bias Ru+Ru and Zr+Zr collisions at $\sqrt{s_{\rm NN}} = 200$ GeV compared to the AMPT-SM model calculations. AMPT-SM model with and without nuclear deformation are close to each other, and the data in the measured p_T range for minimum-bias isobar collisions at $\sqrt{s_{\rm NN}} = 200$ GeV.

Table 1: Parameter set for various deformation configurations of the Ru and Zr nuclei in the AMPT model

Parameter	**Default**		**Deformed**	
System	Ru	Zr	Ru	Zr
R_0	5.096	5.096	5.090	5.090
a	0.540	0.540	0.460	0.520
β_2	0.000	0.000	0.162	0.060
β_3	0.000	0.000	0.000	0.200

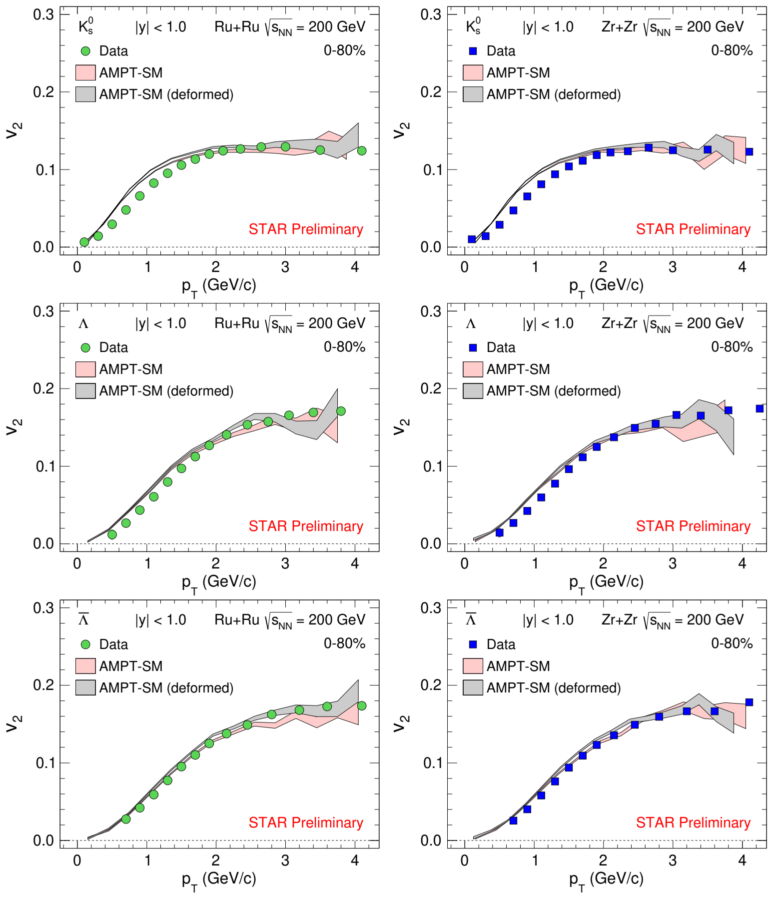

Figure 7: v_2 as a function of p_T for strange hadrons at mid-rapidity in minimum bias Ru+Ru and Zr+Zr collisions at $\sqrt{s_{\mathrm{NN}}}$ = 200 GeV compared to the AMPT model calculations [20, 21]. The error bars represent statistical and systematic uncertainties added in quadrature.

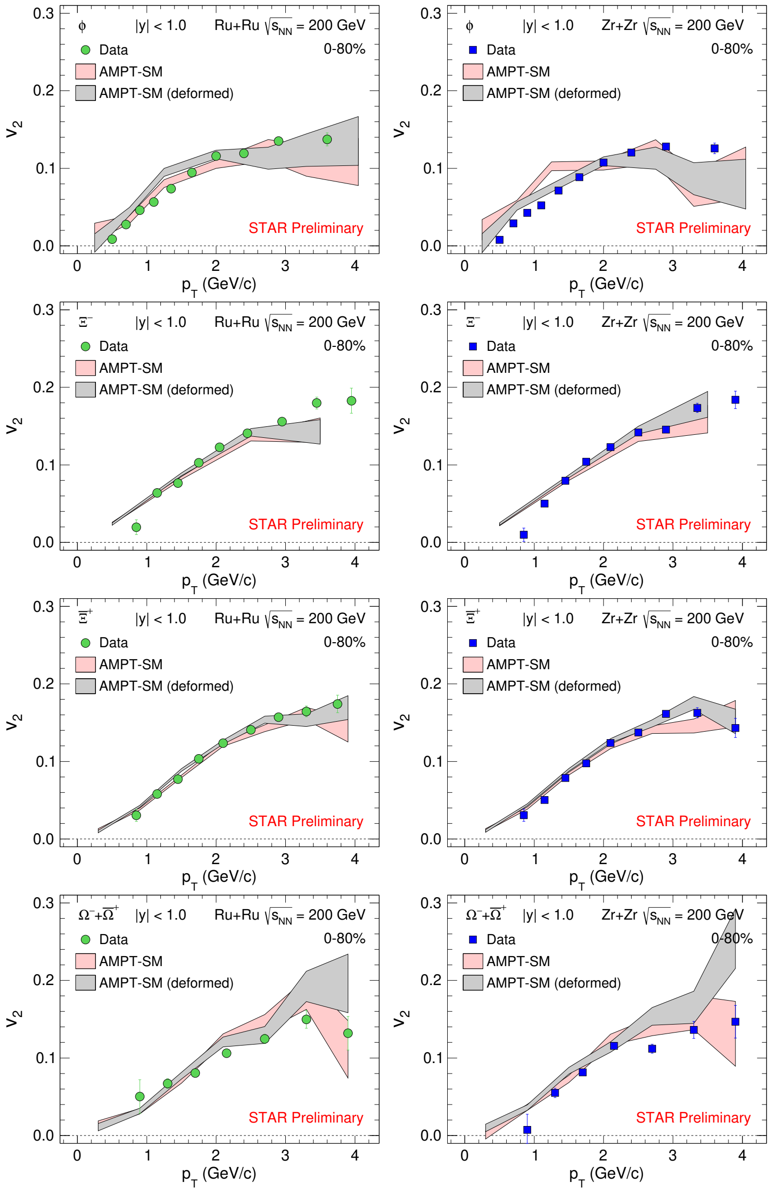

Figure 8: v_2 as a function of p_T for multi-strange hadrons at mid-rapidity in minimum bias Ru+Ru and Zr+Zr collisions at $\sqrt{s_{\rm NN}}$ = 200 GeV compared to the AMPT model calculations [20, 21]. The error bars represent statistical and systematic uncertainties added in quadrature.

4 Summary

We reported transverse momentum dependence of elliptic flow of K_s^0, Λ, $\bar{\Lambda}$, ϕ, Ξ^-, $\overline{\Xi}^+$, and Ω^-+$\overline{\Omega}^+$ at mid-rapidity in Ru+Ru and Zr+Zr collisions at $\sqrt{s_{\rm NN}}$ = 200 GeV for minimum bias (0-80%) and in three centrality intervals (0-10%, 10-40%, and 40-80%). A clear centrality dependence of v_2 is observed in the isobar collisions. We observed a particle mass hierarchy of v_2, which suggests hydrodynamic behavior at low p_T. A baryon-meson splitting of v_2 at intermediate p_T is also observed. The elliptic flow of strange and multi-strange hadrons follows the number of constituent quark scaling, further indicating quark coalescence as the dominant particle production mechanism and the collectivity of the medium. The ratio of p_T-integrated v_2 for strange hadrons between the two isobar collisions shows a deviation from unity, which indicates different intrinsic nuclear structures of the two isobars. We observed a system size dependence of the v_2. The AMPT-SM model, with and without nuclear deformation, provides a good description of the data within the measured p_T range for minimum-bias isobar collisions at $\sqrt{s_{\rm NN}}$ = 200 GeV. These measurements are helpful to shed light on the effect of deformation and collision geometry on anisotropic flow of particle production in relativistic heavy-ion collisions.

References

[1] Shuryak, E.V. Quark-gluon plasma and hadronic production of leptons, photons and psions. Phys. Lett. B **1978**, 78, 150-153, doi:10.1016/0370-2693(78)90370-2.

[2] Cleymans J.; Gavai R.V.; Suhonen E. Quarks and gluons at high temperatures and densities. Phys. Rep. **1986**, 130, 217-292, doi:10.1016/0370-1573(86)90169-9.

[3] Karsch F. Lattice results on QCD thermodynamics. Nucl. Phys. A **2002**, 698, 199-208, doi:10.1016/S0375-9474(01)01365-3.

[4] Arsene I. *et al.* Quark-gluon plasma and color glass condensate at RHIC? The perspective from the BRAHMS experiment. Nucl. Phys. A **2005**, 757, 1-27, doi:10.1016/j.nuclphysa.2005.02.130.

[5] Back B.B. *et al.* The PHOBOS perspective on discoveries at RHIC. Nucl. Phys. A **2005**, 757, 28-101, doi:10.1016/j.nuclphysa.2005.03.084.

[6] Adams J. *et al.* Experimental and theoretical challenges in the search for the quark-gluon plasma: The STAR Collaboration's critical assessment of the evidence from RHIC collisions. Nucl. Phys. A **2005**, 757, 102-183, doi:10.1016/j.nuclphysa.2005.03.085.

[7] Adcox K. *et al.* Formation of dense partonic matter in relativistic nucleus-nucleus collisions at RHIC: Experimental evaluation by the PHENIX Collaboration. Nucl. Phys. A **2005**, 757, 184-283, doi:10.1016/j.nuclphysa.2005.03.086.

[8] Aamodt K. *et al.* Elliptic Flow of Charged Particles in Pb-Pb Collisions at $\sqrt{s_{\rm NN}}$ = 2.76 TeV. Phys. Rev. Lett. **2010**, 105, 252302, doi:10.1103/PhysRevLett.105.252302.

[9] Chatrchyan S. *et al.* Measurement of the pseudorapidity and transverse momentum dependence of the elliptic flow of charged particles in lead-lead collisions at $\sqrt{s_{\rm NN}}$ = 2.76 TeV with the ATLAS detector. Phys. Lett. B **2012**, 707, 330-348, doi:10.1016/j.physletb.2011.12.056.

[10] Aad G. *et al.* Measurement of the elliptic anisotropy of charged particles produced in PbPb collisions at $\sqrt{s_{\rm NN}}$ = 2.76 TeV. Phys. Rev. C **2013**, 87, 014902, doi:10.1103/PhysRevC.87.014902.

[11] Poskanzer A.M.; Voloshin S.A. Methods for analyzing anisotropic flow in relativistic nuclear collisions. Phys. Rev. C **1998**, 58, 1671, doi:10.1103/PhysRevC.58.1671.

[12] Bass S.A. *et al.* Signatures of quark-gluon plasma formation in high energy heavy-ion collisions: a critical review. J. Phys. G **1999**, 25, R1-R57, doi:10.1088/0954-3899/25/3/013.

[13] Abdallah M.S. *et al.* Search for the chiral magnetic effect with isobar collisions at $\sqrt{s_{\rm NN}}$ = 200 GeV by the STAR Collaboration at the BNL Relativistic Heavy Ion Collider. Phys. Rev. C **2022**, 105, 014901, doi:10.1103/PhysRevC.105.014901.

[14] Adams J. *et al.* Multistrange Baryon Elliptic Flow in Au + Au Collisions at $\sqrt{s_{\rm NN}}$ = 200 GeV. Phys. Rev. Lett. **2005**, 95, 122301, doi:10.1103/PhysRevLett.95.122301.

[15] Adamczyk L. *et al.* Elliptic flow of identified hadrons in Au+Au collisions at $\sqrt{s_{\rm NN}}$ = 7.7-62.4 GeV. Phys. Rev. C **2013**, 88, 014902, doi:10.1103/PhysRevC.88.014902.

[16] Abdallah M.S. *et al.* Search for the chiral magnetic effect with isobar collisions at $\sqrt{s_{\rm NN}}$ = 200 GeV by the STAR Collaboration at the BNL Relativistic Heavy Ion Collider. Phys. Rev. C **2022**, 105, 014901, doi:10.1103/PhysRevC.105.014901.

[17] Abelev B.I. *et al.* Centrality dependence of charged hadron and strange hadron elliptic flow from $\sqrt{s_{\rm NN}}$ = 200 GeV Au+Au collisions. Phys. Rev. C **2008**, 77, 054901, doi:10.1103/PhysRevC.77.054901.

[18] Abelev B.I. *et al.* Charged and strange hadron elliptic flow in Cu + Cu collisions at $\sqrt{s_{\mathrm{NN}}} = 62.4$ and 200 GeV. Phys. Rev. C **2010**, 81, 044902, doi:10.1103/PhysRevC.81.044902.

[19] Abdallah M.S. *et al.* Azimuthal anisotropy measurements of strange and multistrange hadrons in U + U collisions at $\sqrt{s_{\mathrm{NN}}} = 193$ GeV at the BNL Relativistic Heavy Ion Collider. Phys. Rev. C **2021**, 103, 064907, doi:10.1103/PhysRevC.103.064907.

[20] Lin Z.-W.; Ko C.M.; Li B.-A.; Zhang B.; Pal S. Multiphase transport model for relativistic heavy ion collisions. Phys. Rev. C **2005**, 72, 064901, doi:10.1103/PhysRevC.72.064901.

[21] Sinha P.; Bairathi V.; Gopal K.; Jena C.; Kabana S. Effect of nuclear structure on particle production in relativistic heavy-ion collisions using a multiphase transport model. Phys. Rev. C **2023**, 108, 024911, doi:10.1103/PhysRevC.108.024911.